The following supplement accompanies the article

Ocean Acoustic Waveguide Remote Sensing (OAWRS) of marine ecosystems

Srinivasan Jagannathan[1], Ioannis Bertsatos[1], Deanelle Symonds[1], Tianrun Chen[1], Hadi Tavakoli Nia[1], Ankita Deepak Jain[1], Mark Andrews[2], Zheng Gong[2], Redwood Nero[3,4], Lena Ngor[1], Mike Jech[4], Olav Rune Godø[5], Sunwoong Lee[1], Purnima Ratilal[2], Nicholas Makris[1,*]

[1]**Department of Mechanical Engineering, Massachusetts Institute of Technology, 77 Massachusetts Avenue, Cambridge, Massachusetts 02139, USA**
[2]**Department of Electrical and Computer Engineering, Northeastern University, 360 Huntington Avenue, Boston, Massachusetts 02115, USA**
[3]**Naval Research Laboratory, 4555 Overlook Avenue SW, Washington DC 20375, USA**
[4]**Northeast Fisheries Science Center, 166 Water Street, Woods Hole, Massachusetts 02543, USA**
[5]**Institute of Marine Research, PO Box 1870, Nordnes, 5817 Bergen, Norway**

*Email: makris@mit.edu

Marine Ecology Progress Series 395:137–160 (2009)

Supplement 1. Predicting fish target strength at low frequencies and estimating physiological parameters from measured target strengths, and experimental design for imaging Antarctic krill

Predicting fish TS at low frequencies and estimating physiological parameters from measured TS

The target strength (TS) of pelagic fish with swimbladders has been studied in detail at the frequencies of conventional fish finding sonar (CFFS; 10 to ~200 kHz) both experimentally and with theoretical models. In this regime, several empirical models relating TS to fish length are available (Love 1971, McClatchie et al. 1996, Ona 2003, Kang et al. 2004, Peltonen & Balk 2005). In contrast, limited fish TS data have been collected at lower frequencies (0.01 to 1 kHz) where OAWRS typically operates and swimbladder resonance is found in many species. Indeed OAWRS is among the first systems to provide data at frequencies ≤1 kHz, where many strong variations in scattering are expected due to swimbladder resonance according to various models (Love 1978, 1993). At such low frequencies, swimbladder scattering becomes effectively omnidirectional so that TS becomes

$$\mathrm{TS} = 10\log_{10}\left(\frac{\Sigma}{4\pi}\right) \tag{1}$$

and the total scattering cross section Σ is directly proportional to the square magnitude of the fish scatter function $S(f)$ and the acoustic wave number via

$$\Sigma = 4\pi\left|\frac{S(f)}{k}\right|^2 \tag{2}$$

which depends on swimbladder shape and material properties of the surrounding fish. According to Love's model (Love 1978), a US Navy standard, the backscattering cross section, related to the total scattering cross section by $\Sigma_{BS} = \Sigma/4\pi$, is given by

$$\Sigma_{BS} = \frac{r^2}{\frac{f_0^2}{f^2}\eta^{-2} + \left(\frac{f_0^2}{f^2} - 1\right)^2} \tag{3}$$

where r is the equivalent swimbladder radius (m), f is the insonifying frequency (Hz), f_0 is the swimbladder's resonance frequency (Hz), and η is a dimensionless damping factor. For swimbladders that can be approximated as prolate spheroids, the resonance frequency is given by

$$f_0 = \kappa\frac{1}{2\pi r}\sqrt{\frac{3\gamma P}{d_f}} \tag{4}$$

where κ is the dimensionless swimbladder correction factor that Weston (1967) obtained using Strasberg's solution for scattering from an oblate spheroid (Strasberg 1953), γ = 1.4 is the ratio of the specific heats of air, P is the ambient pressure (Pa), and d_f is the fish flesh density (kg m^{-3}) (e.g. for Atlantic herring d_f = 1071 kg m^{-3}; Nero et al. 2004). The damping factor η is obtained from

$$\frac{1}{\eta} = \frac{2\pi r f^2}{f_0 c} + \frac{\xi}{\pi r^2 f_0 d_f} \tag{5}$$

where c is the speed of sound in water (m s^{-1}) and ξ is the viscosity of the fish flesh (Pa s) (e.g. empirical value for Atlantic herring: ξ = 50 Pa s; Nero et al. 2004).

The swimbladder correction term (Weston 1967) is

$$\kappa = \frac{\sqrt{2}(1-\varepsilon^2)^{1/4}}{\varepsilon^{1/3}}\left\{\ln\left[\frac{1+\sqrt{1-\varepsilon^2}}{1-\sqrt{1-\varepsilon^2}}\right]\right\}^{-1/2} \tag{6}$$

where the eccentricity ε is the ratio of the minor to major axis of a prolate spheroid.

The volume of the swimbladder is assumed to follow Boyle's Law so that

$$P_0 V_0 = P_z V_z \tag{7}$$

where (P_0, V_0) are the ambient pressure and volume at zero depth, and (P_z, V_z) are the pressure and volume at any depth z. For a prolate spheroid, volume is related to the semi-major axis a and semi-minor axis b by

$$V(z) = \frac{4}{3}\pi a^2(z) b \tag{8}$$

Fish TS is then modeled (Figs. 5, 6, 8, 10, 12, 14, 16 in the

main paper) by assuming the prolate spheroid swimbladder has a major axis that is a constant percentage of total fish length, usually 26 to 33% (Gorska & Ona 2003, Nero et al. 2004). Swimbladder volume is assumed to only change through variation in minor axis (Blaxter 1979, Ona 1990, 2003) due to physical constraints in fish anatomy. Given fish length and depth distribution, target strength can be parameterized by a single parameter, swimbladder volume or equivalently neutral buoyancy depth. For OAWRS 2003 analysis, fish length distributions were determined from overnight *in situ* measurements of individual fish. Measurements were made by CFFS at 38 kHz in the vicinity of the shoals imaged earlier the same day. These TS measurements were then used to calculate the fish mean length, which was found to be approximately 28.6 cm within the OAWRS imaged shoals (McClatchie et al. 1996). Fish depth distribution was also determined from CFFS echograms. For OAWRS 2006, fish length distributions and swimbladder geometries were also obtained from concurrent trawl samples.

The expansion ratio of the minor axis at the surface, $a(0)/a(z_{nb})$, is shown for a range of neutral buoyancy depths z_{nb} typical of physostome fish (Fig. S1). For example, a physostome at the surface would have to take in an amount of air corresponding to a doubling of its swimbladder minor axis to achieve neutral buoyancy at a depth of 30 m. However, neutral buoyancy in physostomes occurs down to 60 m depth (Thorne & Thomas 1990) for which gulping of air is an unlikely mechanism. The neutral buoyancy depth of 78 m, which we obtain by fitting the OAWRS 2003 data with the Love model (Fig. 5 in the main paper), suggests that physostome fish such as herring should have mechanisms either for building up gas in their swimbladder, e.g. gas-producing bacteria in their digestive tract, or for damping which lower and spread the resonance and have shallower neutral buoyancy depth.

A shoal will host herring of variable satiety since swimbladder gas content will vary from diffusive loss or gas-production gain mechanisms so that a system making measurements only above 1.0 kHz would not likely be able to determine the corresponding distribution of neutral buoyancy depths within a shoal. Measurements over a range of frequencies at and below resonance for all physiologically plausible neutral buoyancy depths would be necessary.

The TS corresponding to the average scattering cross section of an individual fish at OAWRS operating frequencies is obtained by calibrating OAWRS fish population densities to those calculated from simultaneous *in situ* CFFS measurements at the spatial locations where simultaneous data in shoals is available (Appendix E in the main paper). OAWRS TS estimation also requires compensating the received sound pressure-levels for (1) 2-way transmission loss in the range-dependent continental-shelf waveguide; (2) the spatially varying resolution footprint of the OAWRS source-receiver system; and (3) source power (Makris et al. 2006, Andrews et al. 2009, Appendix A in the main paper).

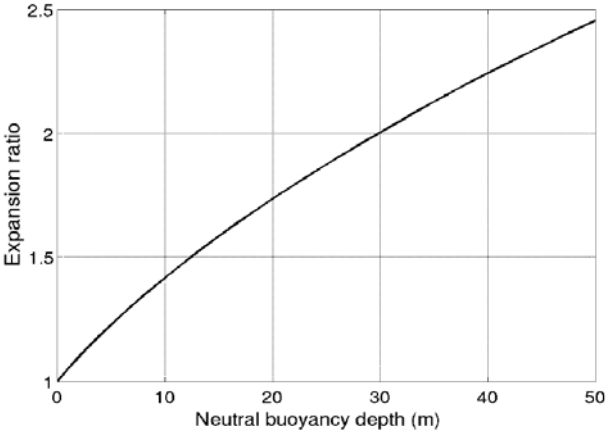

Fig. S1. Expansion ratio of the swimbladder minor axis at the surface as a function of neutral buoyancy depth

For useful concepts about scattering at, or near, swimbladder resonance see Nero & Huster (1996; salmon), Love (1993; blue whiting), Nero et al. (1998; Pacific hake) and Nero et al. (2004; Atlantic herring), where scattering responses of fish at 100 Hz to 5000 Hz were fit to Love's model.

Experimental design for imaging Antarctic krill

In the cold waters of the Antarctic, the increasing hydrostatic pressure with depth leads to a sound speed minimum near the sea surface (Urick 1983), so that sound rays are refracted towards the water–air boundary (Officer 1958, Clay & Medwin 1977, Urick 1983, Brekhovskikh & Lysanov 1991, Jensen et al. 2000). Upward refraction of sound is observed even in summer, when the upper water column is well mixed with a uniform sound speed structure (Fig. S2; Enrico et al. 2003, Argo Database 2009). This makes it possible to design an OAWRS system that channels sound in propagation paths that do not interact with the seafloor, but only the ocean–atmosphere interface (Urick 1983), forming refract-surface reflect (RSR) ray paths as shown in Fig. S2. Since krill are mainly found in the upper water column (<100 m) (Hamner et al. 1983, Lascara et al. 1999, Brierley & Watkins 2000, Brierley et al. 2002), these RSR paths will insonify the krill well with minimal bottom interference.

Given sound speed structure and source depth, it is possible to determine the 'vertex' of an RSR ray path, i.e. the depth where the ray turns from downward to upward refracting (Fig. S2). By choosing a 50 m source depth, and confining the angle of transmission with respect to the horizontal to within $\theta = \pm 5.2°$ in winter and $\theta = \pm 2.5°$ in summer, it is possible to restrict insonification to the top 100 m of the water column. Such beaming of sound requires a source array with a mainlobe width of θ and sidelobe levels that are some orders of magnitude (50 dB in our simulations) lower than the mainlobe level to avoid seafloor interaction. This simple design ensures propagation paths with very little bottom interference and enables OAWRS to detect krill swarms because significant bottom interaction only occurs when propagation angles exceed ±7° in shallow (200 m; Fig. S2), and ±13° in deeper waters (2000 m), with respect to the horizontal.

Angular fluctuations of the source array due to pitch of the source ship may also need to be considered. To minimize bottom interference in the propagation path, maximum angular fluctuations should be constrained to 2° and 8° in winter, and to 4.5° and 10.5° in summer, for shallow and deep water environments, respectively If angular fluctuations exceed the above values, OAWRS imaging of the smaller, 2 cm krill will be severely affected. However, the larger, 3 to 4 cm krill will still be imaged with a dynamic range of at least 15 dB (Fig. 19 in the main paper), for typical swarm densities.

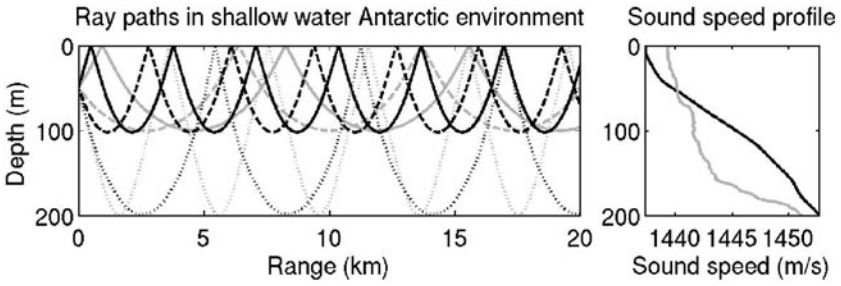

Fig. S2. OAWRS detection of Antarctic krill employs ray paths and the sound speed profile of the Antarctic environment (Chen 2008). The vertical source array of an OAWRS system is centered at 50 m depth and the total water depth is 200 m. Rays within the array mainlobe beam are bounded by the solid and dashed lines and follow RSR paths that can image krill at long ranges. The array mainlobe is designed to be ±5.2° in winter (black lines), and ±2.5° in summer (grey lines). Rays at angles that exceed ±7° (e.g. black dotted lines) are in the much weaker array sidelobes and follow surface-reflected bottom-reflected paths that are contaminated with seafloor scattering returns in shallow water. The figure is not to scale

LITERATURE CITED

Andrews M, Chen T, Ratilal P (2009) Empirical dependence of acoustic transmission scintillation statistics on bandwidth, frequency, and range in New Jersey continental shelf. J Acoust Soc Am 125:111–124

Argo Database (2009) International Argo Project. Accessed 20 May 2009. www.argo.ucsd.edu, http://argo.jcommops.org.

Blaxter JHS (1979) The herring swimbladder as a gas reservoir for the acoustico-lateralis system. J Mar Biol Assoc UK 59:1–10

Brekhovskikh LM, Lysanov YuP (1991) Fundamentals of ocean acoustics. In: Felsen LB (ed) Wave phenomena. Springer-Verlag, Heidelberg

Brierley AS, Watkins JL (2000) Effect of sea ice cover on swarming behaviour of Antarctic krill, *Euphasia superba.* Can J Fish Aquat Sci 57(Suppl 3):24–30

Brierley AS, Fernandes PG, Brandon MA, Armstrong F and others (2002) Antarctic krill under sea ice: elevated abundance in a narrow band just south of ice edge. Science 295:1890–1892

Chen T (2008) Mean, variance, and temporal coherence of the 3D acoustic field forward propagated through random inhomogeneities in continental-shelf and deep ocean waveguides. PhD dissertation, Massachusetts Institute of Technology, Cambridge, MA

Clay CS, Medwin H (1977) Acoustical oceanography: principles and applications. John Wiley & Sons, New York

De Marinis E, Picco P, Meloni R (2003) Monitoring polynyas with Ocean Acoustic Tomography: a feasibility study in Terra Nova Bay. Antarct Sci 15:63–75

Gorska N, Ona E (2003) Modeling the effect of swimbladder compression on the acoustic backscattering from herring at normal or near-normal dorsal incidences. ICES J Mar Sci 60:1381–1391

Hamner WM, Hamner PP, Strand SW, Gilmer RW (1983) Behavior of Antarctic krill, *Euphausia superba*: chemoreception, feeding, schooling and molting. Science 220: 433–435

Jensen FB, Kuperman WA, Porter MB, Schmidt H (2000) Computational ocean acoustics. Springer-Verlag, New York

Kang D, Sadayasu K, Mukai T, Iida K, Hwang D, Sawada K, Miyashita K (2004) Target strength estimation of black porgy *Acanthopagrus schlegeli* using acoustic measurements and a scattering model. Fish Sci 70:819–828

Lascara CM, Hofmann EE, Ross RM, Quetin LB (1999) Seasonal variability in the distribution of Antarctic krill, *Euphausia superba*, west of the Antarctic peninsula. Deep-Sea Res I 46:951–984

Love RH (1971) Dorsal-aspect target strength of an individual fish. J Acoust Soc Am 49:816–823

Love RH (1978) Resonant acoustic scattering by swimbladder-bearing fish. J Acoust Soc Am 64:571–580

Love RH (1993) A comparison of volume scattering strength data with model calculations based on quasisynoptically collected fishery data. J Acoust Soc Am 94:2255–2268

Makris NC, Ratilal P, Symonds DT, Jagannathan S, Lee S, Nero RW (2006) Fish population and behavior revealed by instantaneous continental shelf-scale imaging. Science 311:660–663

McClatchie S, Alsop J, Coombs RF (1996) A re-evaluation of relationships between fish size, acoustic frequency, and target strength. ICES J Mar Sci 53:780–791

Nero RW, Huster ME (1996) Low-frequency acoustic imaging of Pacific salmon on the high seas. Can J Fish Aquat Sci 53:2513–2523

Nero RW, Thompson CH, Love R (1998) Low-frequency acoustic measurements of Pacific hake, *Merluccius productus*, off the west coast of the United States. Fish Bull 96:329–343

Nero RW, Thompson CH, Jech JM (2004) *In situ* acoustic estimates of the swimbladder volume of Atlantic herring (*Clupea harengus*). ICES J Mar Sci 61:323–337

Officer CB (1958) Introduction to the theory of sound transmission. McGraw-Hill, New York

Ona E (1990) Physiological factors causing natural variations in acoustic target strength of fish. J Mar Biol Assoc UK 70:107–127

Ona E (2003) An expanded target-strength relationship for herring. ICES J Mar Sci 60:493–499

Peltonen H, Balk H (2005) The acoustic target strength of herring (*Clupea harengus* L.) in the Northern Baltic Sea. ICES J Mar Sci 62:803–808

Strasberg M (1953) The pulsation frequency of nonspherical gas bubbles in liquids. J Acoust Soc Am 25:536–537

Thorne RE, Thomas GL (1990) Acoustic observations of gas-bubble release by Pacific herring (*Clupea harengus pallasi*). Can J Fish Aquat Sci 47:1920–1928

Urick RJ (1983) Principles of underwater sound, 3rd edn. McGraw-Hill, New York